

The Aharonov-Bohm effect in mesoscopic Bose-Einstein condensates

Tobias Haug,¹ Hermanni Heimonen,¹ Rainer Dumke,^{1,2,3} Leong-Chuan Kwek,^{1,3,4,5} and Luigi Amico^{1,3,6,7,8}

¹Centre for Quantum Technologies, National University of Singapore, 3 Science Drive 2, Singapore 117543, Singapore

²Division of Physics and Applied Physics, Nanyang Technological University, 21 Nanyang Link, Singapore 637371, Singapore

³MajuLab, CNRS-UNS-NUS-NTU International Joint Research Unit, UMI 3654, Singapore

⁴Institute of Advanced Studies, Nanyang Technological University, 60 Nanyang View, Singapore 639673, Singapore

⁵National Institute of Education, Nanyang Technological University, 1 Nanyang Walk, Singapore 637616, Singapore

⁶Dipartimento di Fisica e Astronomia, Via S. Sofia 64, 95127 Catania, Italy

⁷CNR-MATIS-IMM & INFN-Sezione di Catania, Via S. Sofia 64, 95127 Catania, Italy

⁸LANEF 'Chaire d'excellence', Université Grenoble-Alpes & CNRS, F-38000 Grenoble, France

(Dated: June 11, 2022)

The Aharonov-Bohm, and its dual, the Aharonov-Casher effects have been extremely fruitful in physics and, nowadays, they are of central importance for quantum technologies. Here, we study the Aharonov-Bohm effect for a Bose-Einstein condensate propagating out of equilibrium along a mesoscopic ring-shaped laser light potential, pierced by an effective magnetic flux. We found how the system experiences a subtle crossover between physical regimes dominated by pronounced interference patterns and others in which the Aharonov-Bohm effect is effectively washed out. We propose various applications for this system.

The Aharonov-Bohm effect is one of the most striking manifestations of quantum mechanics: Due to phase shifts of the wave function, specific interference effects arise when charged particles enclose a region with a non vanishing magnetic field[1]. Besides to have been of pivotal importance in foundational aspects of quantum physics[1–4] and many-body quantum physics[5–9], the Aharonov-Bohm effect has been influential in the very definition of more applicative ramifications of physical science, like mesoscopic physics, quantum electronics, molecular electronics etc.[10–13], with remarkable spin-off to conceive and realize specific quantum devices that have been of ready-use in quantum technology[13–19].

An electronic fluid confined in a ring-shaped wire pierced by a magnetic flux is the typical configuration employed to study the Aharonov-Bohm effect. In this way, a matter-wave interferometer can be realized: The current through the ring-shaped quantum system displays characteristic oscillations depending on the imparted magnetic flux. Neutral particles with magnetic moments display interference effects with a similar Aharonov-Bohm logic[20].

New perspectives to study the transport through quantum matter have been provided by very recent studies inherent to the physics of ultracold atoms[21–24]. This way, the system physical conditions implied by the carrier statistics, particle-particle interactions and circuits spatial configuration can be adjusted to a degree that was very hard, if not impossible, to achieve so far.

In this paper, we study the Aharonov-Bohm effect in a mesoscopic ring-shaped bosonic condensate pierced by a synthetic magnetic flux[25]. We exploit Atomtronics as the logical platform to study such systems, a platform that is also ideally suited for experimental analysis[26]: In our scheme, the bosonic fluid is injected from a ‘source’ lead, propagates along the ring, and it is collected in a ‘drain’ lead. We see that, depending on the ring-lead coupling, boson-boson interactions and particle statistics, the system displays qualitatively distinct non-equilibrium regimes characterized by different re-

sponse of the interference pattern established by the effective gauge field. We shall see that our bosonic system, indeed, displays very distinctive features compared with the corresponding fermionic system. Finally, we exploit our findings as basic principles for conceiving new atomtronic quantum devices.

The system dynamics– The Bose-Hubbard Hamiltonian

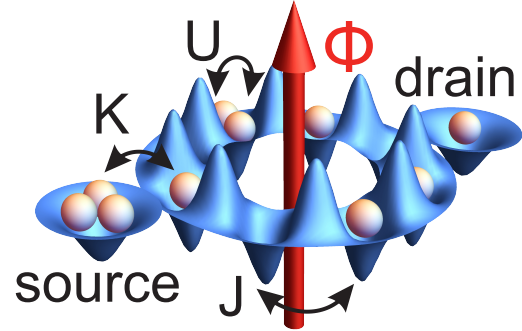


FIG. 1. Atomtronic setup consisting of a superfluid condensate in a ring lattice with two attached leads. The dynamics is controlled by Aharonov-Bohm flux Φ and ring-lead coupling K . Particles tunnel between ring sites with rate J and particles interact on-site with strength U .

$\mathcal{H} = \mathcal{H}_r + \mathcal{H}_l$ describes the system consisting of a ring with an even number of lattice sites L and two leads (see Fig.1). The ring is given by

$$\mathcal{H}_r = - \sum_{j=0}^{L-1} \left(J e^{i2\pi\Phi/L} \hat{a}_j^\dagger \hat{a}_{j+1} + \text{H.C.} \right) + \frac{U}{2} \sum_{j=0}^{L-1} \hat{n}_j (\hat{n}_j - 1), \quad (1)$$

where \hat{a}_j and \hat{a}_j^\dagger are the annihilation and creation operator at site j , $\hat{n}_j = \hat{a}_j^\dagger \hat{a}_j$ is the particle number operator, J is the intra-ring hopping, U is the on-site interaction between particles and Φ is the total flux through the ring. Periodic boundary conditions are applied: $\hat{a}_L^\dagger = \hat{a}_0^\dagger$.

The two leads dubbed source (S) and drain (D) consist of a

single site each. They couple symmetrically at opposite sites to the ring with coupling strength K

$$\mathcal{H}_1 = -K(\hat{a}_S^\dagger \hat{a}_0 + \hat{a}_D^\dagger \hat{a}_{L/2} + \text{H.C.}), \quad (2)$$

where \hat{a}_S^\dagger and \hat{a}_D^\dagger are the creation operators of source and drain respectively.

The system is initially prepared with all particles in the source and the dynamics is strongly affected by the lead-ring coupling. We calculate the state at time t with $|\Psi(t)\rangle = e^{-i\mathcal{H}t} |\Psi(0)\rangle$. We investigate the expectation value of the density in source and drain over time, which for the source is calculated as $n_{\text{source}}(t) = \langle \Psi(t) | \hat{a}_S^\dagger \hat{a}_S | \Psi(t) \rangle$ and similar for the drain. In the weak-coupling regime $K/J \ll 1$, the lead-ring coupling is slow compared to the dynamics inside the ring. In this regime, the condensate mostly populates the drain and source, leaving the ring nearly empty. As a result, the scattering due to on-site interaction U has a negligible influence on the dynamics. The transfer rate through the ring is strongly

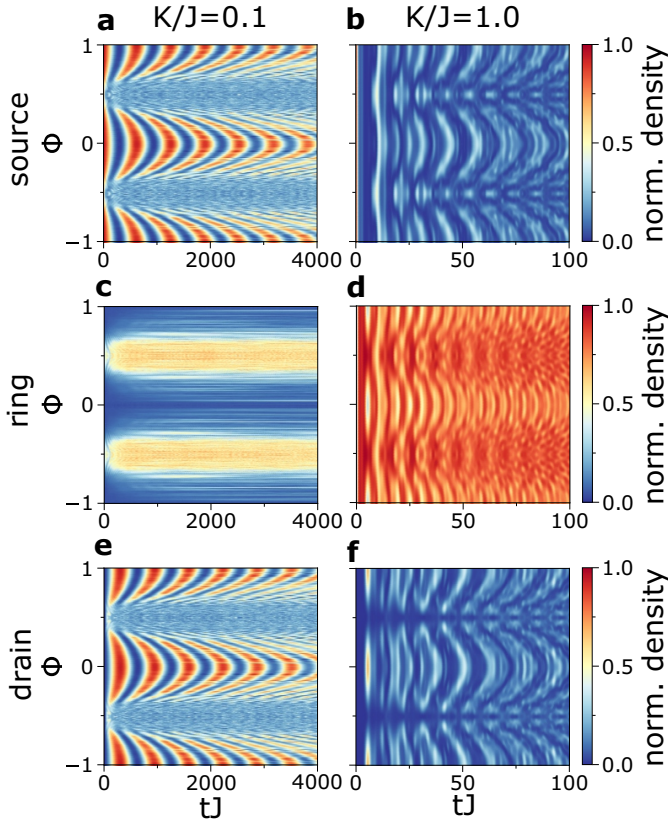


FIG. 2. Time evolution of density in source **a,b**), ring **c,d**) and drain **e,f**) plotted against flux Φ . **a,c,e**) weak ring-lead coupling $K/J = 0.1$ (on-site interaction $U/J = 5$). **b,d,f**) strong ring-lead coupling $K/J = 1$ ($U/J = 0.2$). The number of ring sites is $L = 14$ with 4 particles initially in the source. The density in the ring is given by $n_{\text{ring}} = 1 - n_{\text{source}} - n_{\text{drain}}$.

influenced by interference, giving rise to regular patterns and a pronounced Aharonov-Bohm effect (Fig.2a,c,e). Close to the degeneracy point the oscillation becomes faster and the ring

populates, resulting in increased scattering and washed-out density oscillations. In the strong-coupling regime $K/J \approx 1$, the lead-ring and the intra-ring dynamics are characterized by the same frequency and cannot be treated separately. In this regime, the condensate is evenly spread both in the leads and in the ring potential (Fig.2b,d,f). Close to $\Phi = 0.5$, the oscillation between source and drain slows down, especially for weak interaction, due to destructive interference.

We find that the dynamics is affected by the parity in half of the number of ring sites $L/2$, which is especially pronounced in the weak-coupling regime as we show in the following. In Fig.3, the density in source and drain is plotted against Φ for odd ($L/2 = 3, 5, 7, \dots$) and even parity ($L/2 = 2, 4, 6, \dots$) for $K/J = 0.1$. Both flux dependence and time scales differ widely for the two parities. We can understand such parity effects in terms of ring-lead resonant and off-resonant coupling, which is similar to the tunneling through a quantum dot[27, 28]. For $\Phi = 0$, all ring modes of the system with odd $L/2$ are out of resonance with the leads, while for $L/2$ even, two ring modes are on resonance. Off-resonant coupling (large enough energy gap between lead and ring modes) does not contribute for even parity as off-resonant ring modes turn out to interfere destructively, while for odd it is a dominant contribution due to constructive interference. As a result, for odd parity the transfer rate is much smaller than in the resonant case for even parity. For the degenerate case $\Phi = 0.5$, odd parity has two ring modes on resonance, while none for even. We observe fast density oscillations (washed out by interaction) for odd, while for even parity there is negligible transfer due to a lack of resonant ring modes and absence of off-resonant coupling. These effects are less visible with strong coupling or many ring sites as the energy gap between ring modes diminishes and many ring modes come into resonance, washing out the difference between the parities. Detailed derivation is found in the supplemental A.4.

The crossover from weak to strong coupling regime for odd parity is plotted in Fig.4. It is marked by a transition from slow to fast oscillations. With stronger lead-ring coupling, additional frequency modes contribute. In the strong-coupling regime, the dynamics depend strongly on interaction, as the density in the ring is large and particles scatter strongly there. In the weak coupling regime the ring population is low and scattering is negligible. The weak coupling regime is therefore unaffected by intermediate on-site interaction.

Finally, to study the properties of a filled ring, in Fig.5 we attach particle reservoirs at the leads and drive a current through the now open system and let it evolve until the steady-state is reached. For no interaction we found a very good agreement with the result of Büttiker et al.[11] (details in supplementary). We discovered that the type of particle (Boson, fermion, anyon) and inter-particle interaction has a profound influence on the Aharonov-Bohm effect. While fermions or non-interacting bosons react strongly to an applied flux, interacting bosons have only weak dependence on the flux. Anyons and fermions have zero current for certain values of flux (at the degenerate points), while the current is always

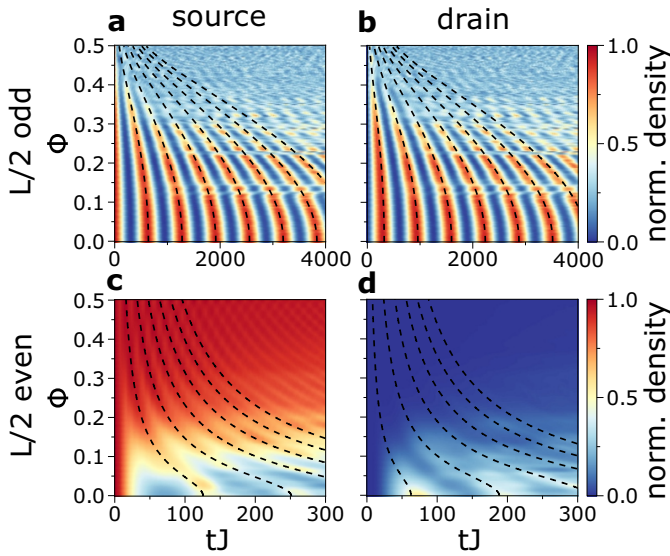


FIG. 3. Density in source and drain against flux Φ for even and odd parity in number of ring sites **a,b**) $L/2 = 7$ ($U/J = 3$) and **c,d**) $L/2 = 8$ ($U/J = 1$). Other parameters are 4 particles and $K/J = 0.1$. The structures around $\Phi = 0.15$ for odd parity are many-body resonances[29]. Dashed line shows analytic derived oscillation period by calculating the coupling of the leads via resonant and off-resonant ring modes similar to concepts known from lead to quantum dot coupling[28]. Details on the analytic result are found in the supplemental (**a,b**) Eq.A.15 and **c,d**) Eq.A.6).

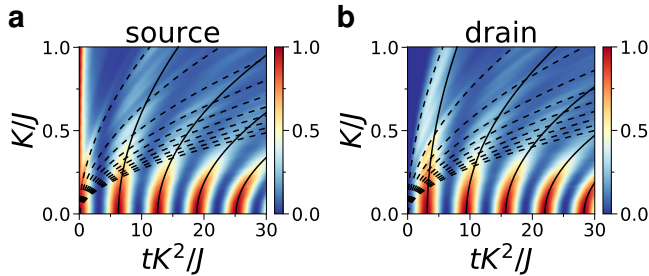


FIG. 4. Density in source **a**) and drain **b**) against ring-lead coupling K/J for $L/2 = 7$, $U/J = 1$. For weak ring-lead coupling only one oscillation mode contributes, whereas for strong coupling additional oscillation modes are excited. The dashed and solid line show the two main modes of oscillation calculated with the same method as in Fig.3 (Eq.A.15).

non-zero for interacting bosons. Remarkably, for interacting bosons in the strong coupling regime the Aharonov-Bohm effect is effectively suppressed[30], whereas some structure in the transmission is observed for weak coupling. In summary, the Aharonov-Bohm effect in the mesoscopic regime does experience a non-trivial cross-over as a function of the ring-lead coupling strength.

Applications– Here we present possible applications based on the physics discussed above.

As first application, we study the atomtronic counterpart of the dc-SQUID: We insert two impurities (with potential offset Δ as defined in supplement) symmetrically in the center of up-

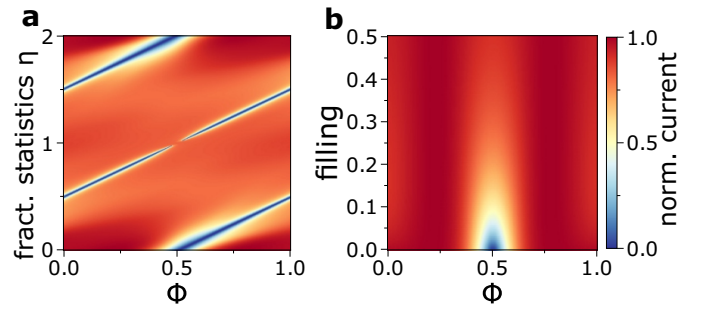


FIG. 5. **a**) Steady-state current for strong-coupling $K/J = 1$ plotted against flux Φ and fractional statistics η ($\eta = \{0, 2\}$ fermions, $\eta = 1$ hard-core bosons, else anyons) for strong source-drain imbalance driving ($f = 1$) and a half-filled system on average. The number of ring sites is $L/2 = 3$ and the on-site interaction is infinite both in leads and ring. Fermions and anyons have zero current at a specific flux, whereas for strongly interacting bosons the current is nearly constant and the Aharonov-Bohm effect suppressed. The anyon statistics shift the minimum of the Aharonov-Bohm interference as the commutation relations introduce an effective flux, which depends on the average number of particles in ring and therefore the number of ring sites. A discontinuity of the minimum is observed for bosons. **b**) Steady state current for hard-core bosons plotted against flux and the filling factor in the leads. With increasing filling, scattering increases and Aharonov-Bohm effect vanishes. For fermions, it is independent of filling (see supplemental). There is a small difference of filling between source and drain of $\Delta n = 0.01$. The steady-state current operator is $j = -iK(\hat{a}_S^\dagger \hat{a}_0 - \hat{a}_0^\dagger \hat{a}_S)$. The expectation value is calculated as $\langle j \rangle = \text{Tr}(j\rho)$ with ρ being the steady-state density matrix. The leads are incoherently coupled to a particle reservoir at the leads with a population imbalance between source and drain. The coupling is assumed to be weak and within the Born-Markov approximation, modeled with the Lindblad Master-equation Eq.A.20 with $\Gamma = 0.5$ as defined in the supplemental.

per and lower arm of the ring. The dependence on Δ is shown in Fig.6a,b. The impurity strength modifies the transfer rate to the drain in a quantitatively similar way as the Aharonov-Bohm flux. However, no destructive interference is observed. This indicates that the impurity influences the dynamics only by scattering incoming particles, but does not imprint a phase shift. Adjusting the strength of the two impurities, instead, we found we can control the source-drain transfer rate.

As a second application, we study the propagation through a quantum dot like structure[27, 31, 32]. This time, the local potential is in only one arm of the ring, but on several consecutive ring sites. We found that distinct transmission minima are displayed (see Fig.6c). Such results indicate that the particle acquires a phase difference while traveling through the ring.

Finally, we investigate the Perfect State Transfer protocol: under a certain coupling configuration, the particles can move from source to drain and vice-versa without dispersion at a fixed rate[33]. The flux dependence of the time evolution of the density is seen in Fig.6d. At $\Phi = 0$ we observe that the density in source and drain oscillates at a constant rate with nearly unit probability. In contrast to weak coupling, the parti-

cles move as a wave packet inside the ring. By tuning the flux, the drain density can be controlled and transmission to the drain becomes zero at the degeneracy point. The setup with

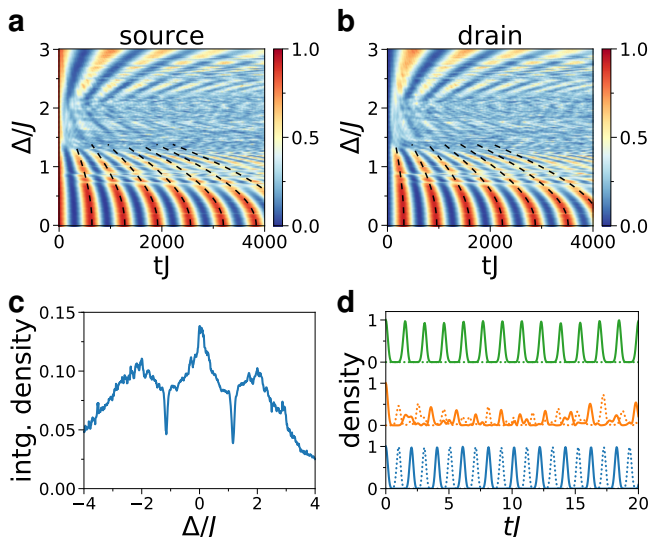


FIG. 6. **a,b**) Density in source and drain plotted against potential barrier placed symmetrically in both arms of the ring with depth Δ . $K/J = 0.1$ and $U/J = 3$ with Bose-Hubbard model. Dashed line indicates a fit with analytic formula for oscillation period used for the flux dependence in Fig.3a,b (Eq.A.15, replace Φ with $\Delta/(2J)$). **c**) Density in drain integrated over a time $t = 10000/J$ for a modified local potential Δ along one arm of the ring. Interference effects cause minima in transmission rate for certain values of Δ . Parameters are 4 particles, $K/J = 1$ and $U/J = 0.1$. **d**) Density in source (solid) and drain (dashed) with $U/J = 5$ and $L = 14$. Couplings are chosen in a specific way such that for $\Phi = 0$ a particle in the source at $t = 0$ will be with unity probability in the drain at $t = 1$. From bottom to top $\Phi = \{0, 0.25, 0.5\}$. Modelled with mean-field interaction in both in ring and leads.

perfect state transfer could realize a switch or quantum interference transistors[34]. By changing the flux, perfect transmission is changed into perfect reflection. We propose to use the high control over the dynamics to create an atomic version of a Elitzur-Vaidman bomb tester, the hallmark example of an interaction-free measurement[35]. The system is prepared with a single particle, the flux set to the degeneracy point and a bomb, which is triggered by a particle passing through one arm of the ring. Only if there is a bomb and it has not been triggered, the particle reaches the drain. This setup has a 50% chance to detect the bomb without detonating it, improving from the 33% efficiency of the photonic implementation.

Acknowledgments. The Grenoble LANEF framework (ANR-10-LABX-51-01) is acknowledged for its support with mutualized infrastructure. We thank National Research Foundation Singapore and the Ministry of Education Singapore Academic Research Fund Tier 2 (Grant No. MOE2015-T2-1-101) for support.

- [1] Y. Aharonov and D. Bohm, Phys. Rev. **115**, 485 (1959).
- [2] S. Olariu and I. I. Popescu, Rev. Mod. Phys. **57**, 339 (1985).
- [3] L. Vaidman, Phys. Rev. A **86**, 040101 (2012).
- [4] A. J. Leggett, Progr. Theoret. Phys. Suppl. **69**, 80 (1980).
- [5] A. Lobos and A. Aligia, Phys. Rev. Lett. **100**, 016803 (2008).
- [6] J. Rincón, A. Aligia, and K. Hallberg, Phys. Rev. B **79**, 035112 (2009).
- [7] P. Shmakov, A. Dmitriev, and V. Y. Kachorovskii, Phys. Rev. B **87**, 235417 (2013).
- [8] O. Hod, R. Baer, and E. Rabani, Phys. Rev. Lett. **97**, 266803 (2006).
- [9] E. Jagla and C. Balseiro, Phys. Rev. Lett. **70**, 639 (1993).
- [10] Y. Gefen, Y. Imry, and M. Y. Azbel, Phys. Rev. Lett. **52**, 129 (1984).
- [11] M. Büttiker, Y. Imry, and M. Y. Azbel, Phys. Rev. A **30**, 1982 (1984).
- [12] R. A. Webb, S. Washburn, C. Umbach, and R. Laibowitz, Phys. Rev. Lett. **54**, 2696 (1985).
- [13] A. Nitzan and M. A. Ratner, Science **300**, 1384 (2003).
- [14] N. Byers and C. Yang, Phys. Rev. Lett. **7**, 46 (1961).
- [15] F. Bloch, Phys. Rev. **166**, 415 (1968).
- [16] L. Gunther and Y. Imry, Solid State Commun. **7**, 1391 (1969).
- [17] A. Bachtold, C. Strunk, J.-P. Salvetat, J.-M. Bonard, L. Forró, T. Nussbaumer, and C. Schönberger, Nature (London) **397**, 673 (1999).
- [18] U. C. Coskun, T.-C. Wei, S. Vishveshwara, P. M. Goldbart, and A. Bezryadin, Science **304**, 1132 (2004).
- [19] D. M. Cardamone, C. A. Stafford, and S. Mazumdar, Nano Lett. **6**, 2423 (2006).
- [20] Y. Aharonov and A. Casher, Phys. Rev. Lett. **53**, 319 (1984).
- [21] D. Papoular, L. Pitaevskii, and S. Stringari, Phys. Rev. Lett. **113**, 170601 (2014).
- [22] A. Li, S. Eckel, B. Eller, K. E. Warren, C. W. Clark, and M. Edwards, Phys. Rev. A **94**, 023626 (2016).
- [23] D. Papoular, L. Pitaevskii, and S. Stringari, Phys. Rev. A **94**, 023622 (2016).
- [24] S. Krinner, D. Stadler, D. Husmann, J.-P. Brantut, and T. Esslinger, Nature (London) **517**, 64 (2015).
- [25] J. Dalibard, F. Gerbier, G. Juzeliūnas, and P. Öhberg, Rev. Mod. Phys. **83**, 1523 (2011).
- [26] L. Amico and A. M. G. Boshier, in *R. Dumke, Roadmap on quantum optical systems*, Vol. 18 (Journal of Optics, 2016) p. 093001.
- [27] J. Wu, B.-L. Gu, H. Chen, W. Duan, and Y. Kawazoe, Phys. Rev. Lett. **80**, 1952 (1998).
- [28] L. Glazman and M. Pustilnik, in *New directions in mesoscopic physics (towards nanoscience)* (Springer, 2003) pp. 93–115.
- [29] M. Sturm, M. Schlosser, R. Walser, and G. Birkel, arXiv:1705.01271.
- [30] A. Tokuno, M. Oshikawa, and E. Demler, Phys. Rev. Lett. **100**, 140402 (2008).
- [31] A. L. Yeyati and M. Büttiker, Phys. Rev. B **52**, R14360 (1995).
- [32] C. Bruder, R. Fazio, and H. Schoeller, Phys. Rev. Lett. **76**, 114 (1996).
- [33] L. Dai, Y. Feng, and L. Kwok, J. Phys. A Math. Theor. **43**, 035302 (2009).
- [34] F. Giazotto, J. T. Peltonen, M. Meschke, and J. P. Pekola, Nat. Phys. **6**, 254 (2010).
- [35] A. C. Elitzur and L. Vaidman, Found. Phys. **23**, 987 (1993).
- [36] T. Prosen, New J. Phys. **10**, 043026 (2008).
- [37] G. Benenti, G. Casati, T. Prosen, D. Rossini, and M. Žnidarič,

Phys. Rev. B **80**, 035110 (2009).

[38] L. Amico, A. Osterloh, and U. Eckern, Phys. Rev. B **58**, R1703 (1998).

[39] C. Guo and D. Poletti, arXiv:1609.07249.

Appendix: Weak coupling

In the following sections, we provide additional results on the dynamics in the ring-lead system. We start the discussion with the weak-coupling limit and the dependence on the ring length L for no interaction. In Fig.7, we plot the dependence on ring length for the two parities $L/2$ odd and even. Both parities have a different dependence on the ring length. For small ring length, a single oscillation between source and drain dominates, while for larger ring length additional frequencies appear. We fit both with analytic solutions.

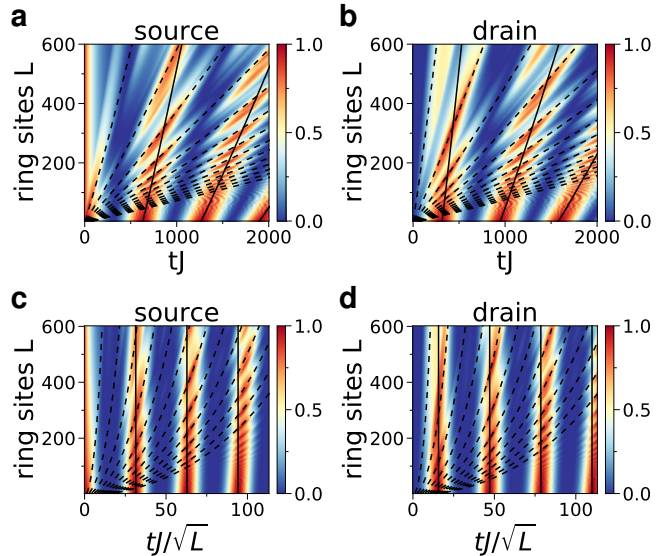


FIG. 7. Density in source and drain against ring length for $K/J = 0.1$, $\Phi = 0$ and parity $L/2$ odd (analytic solution with Eq.A.15) and $L/2$ even (Eq.A.9 (solid) and A.6(dashed)).

Next, we focus on the ring length for the parity $L/2$ even in Fig.8 for different values of flux. For non-zero flux, we observed oscillations in the source only for small flux. For larger ring lengths, oscillations appear for any flux.

Now, we investigate the flux dependence of parity $L/2$ odd in Fig.9.

Next, we investigate the flux dependence for no interaction. For odd parity $L/2 = 7$ in Fig.10 we plot the full range and a zoom in close to the degeneracy point. Close to the degeneracy point, the oscillation become very fast. Here, we observe a characteristic beating pattern, which is plotted as a solid line.

For odd parity $L/2 = 8$ we plot the flux dependence in Fig.11. The oscillation in source disappear close to the degeneracy point.

Appendix: Weak to strong coupling

In this section we investigate the transition from weak to strong coupling.

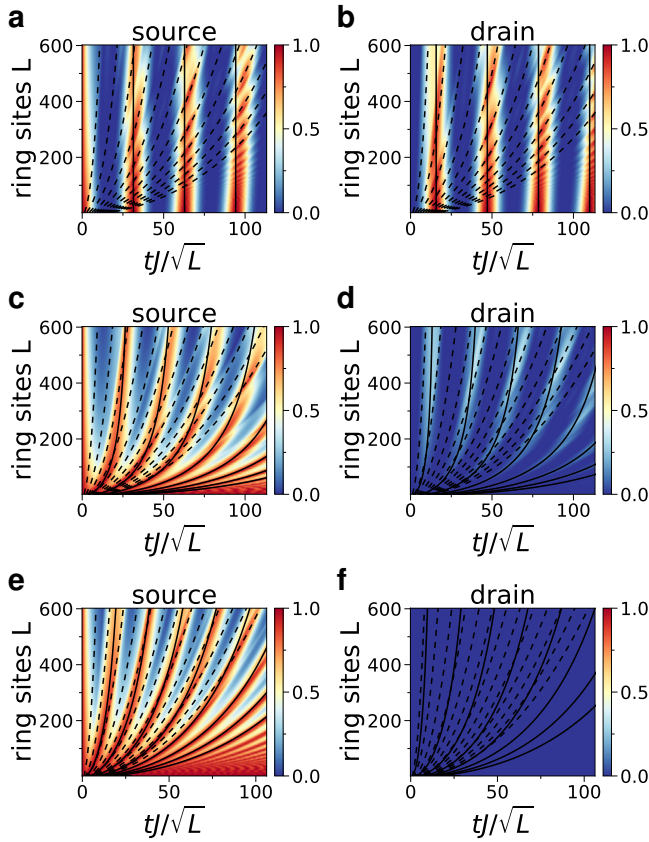


FIG. 8. Density in source and drain against ring length for $K/J = 0.1$ and parity $L/2$ even for $\Phi = \{0, 0.25, 0.5\}$. Solid line is Eq. A.6 and dashed A.9.

We plot the time evolution against ring-lead coupling K for different values of Φ and parity in Fig. 12. With increasing ring-lead coupling, we observe a transition from a single oscillation to more oscillation frequencies. The main oscillation frequency is fitted analytically and is still visible even for strong coupling. We observe for strong coupling characteristic beating patterns, which we can fit analytically.

We plot the ring-lead coupling K for different U/J in Fig. 13. For weak-coupling K/J , we observe source drain oscillation which are nearly independent of U/J , as the ring population in the weak-coupling limit is low, suppressing particle-particle scattering. With increasing K/J , we notice faster oscillation patterns. They smear out with increasing interaction as the ring fills up for stronger ring-lead coupling.

Appendix: Strong coupling

Next, we discuss the strong-coupling limit $K/J = 1$ and many ring sites. In Fig. 14, we plot the number of ring sites against the time evolution. Note that there is no parity effect visible. The data can be described by traveling wave packets, and does not have a cosine like solutions as in the other cases.

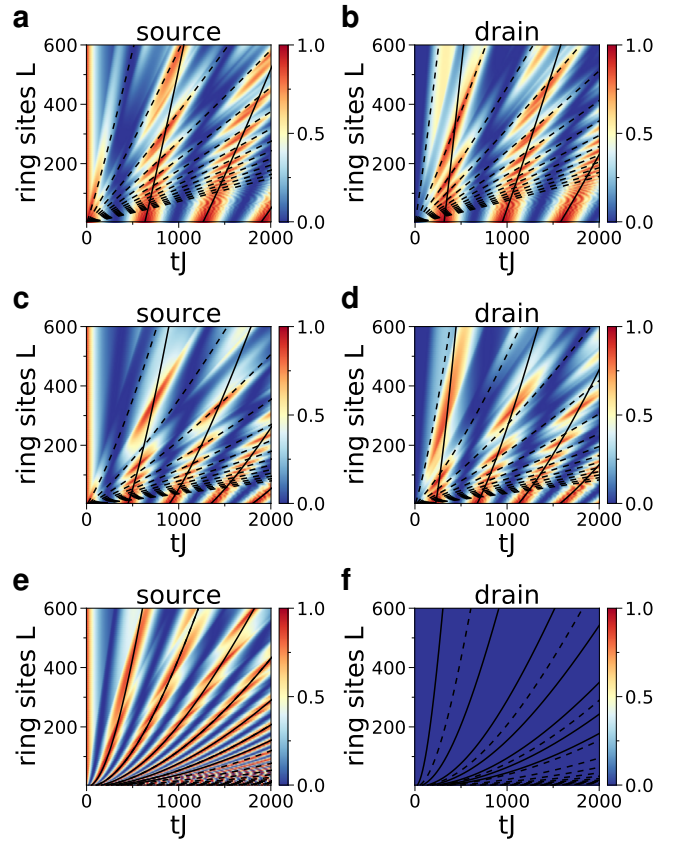


FIG. 9. Density in source and drain against ring length for $K/J = 0.1$ and parity $L/2$ odd for $\Phi = \{0, 0.25, 0.5\}$. Analytic solution in solid and dashed with Eq. A.15.

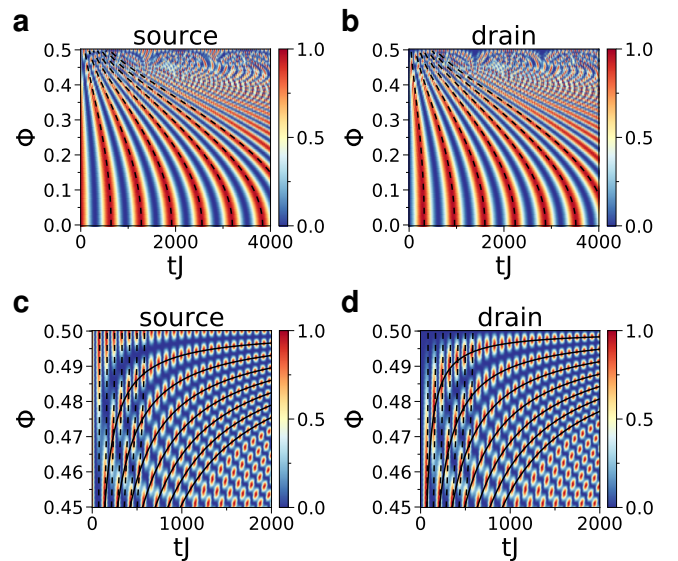


FIG. 10. Density in source and drain against flux for $K/J = 0.1$ and $L/2 = 7$. Top graphs show full flux range, bottom a close up towards $\Phi = 0.5$. Analytic solution in solid and dashed with Eq. A.15.

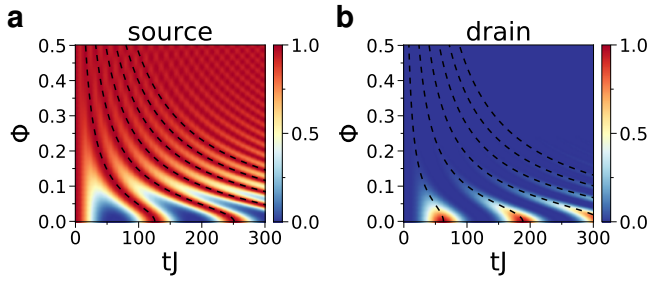


FIG. 11. Density in source and drain against flux for $L/2 = 8$ and $K/J = 0.1$. Analytic solution as dashed lines with Eq.A.6.

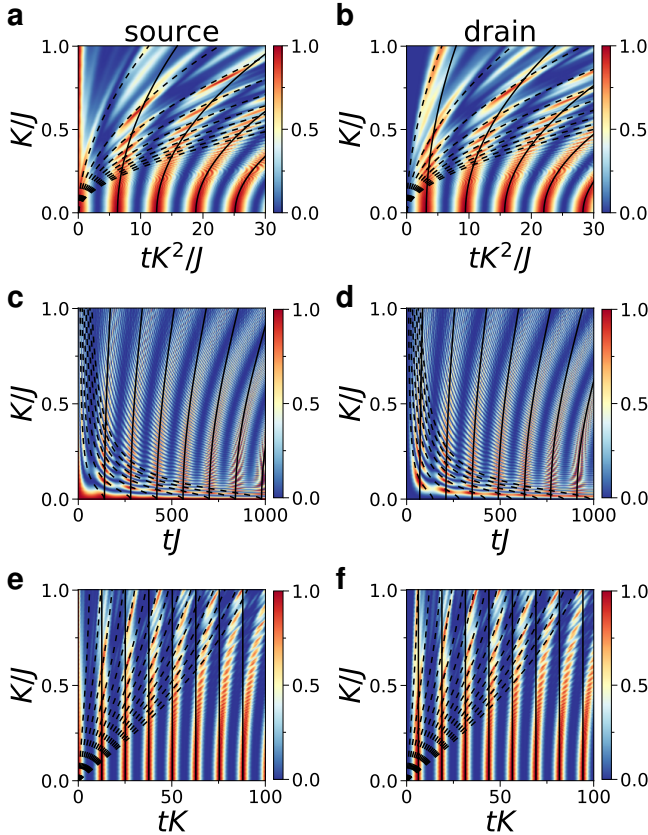


FIG. 12. Density in source and drain against K/J for $L/2 = 7$, **a,b**) $\Phi = 0$ and **c,d**) $\Phi = 0.45$, and **e,f**) $L/2 = 8$ with $\Phi = 0$. Analytic solution for odd $L/2 = 7$ with Eq.A.15, and for even $L/2 = 8$ with Eq.A.9 (solid) and A.6 (dashed).

Next, we go to a mesoscopic number of ring sites, and plot the flux Φ against time for the two parities in Fig.15. In both cases, we observe a beating pattern for flux close to $\Phi = 0.5$, which can be described by the analytic solutions quite well.

Appendix: Potential barrier

Next, we study the effect of a potential barriers in the weak-coupling regime. By introducing two potential barriers Δ sym-

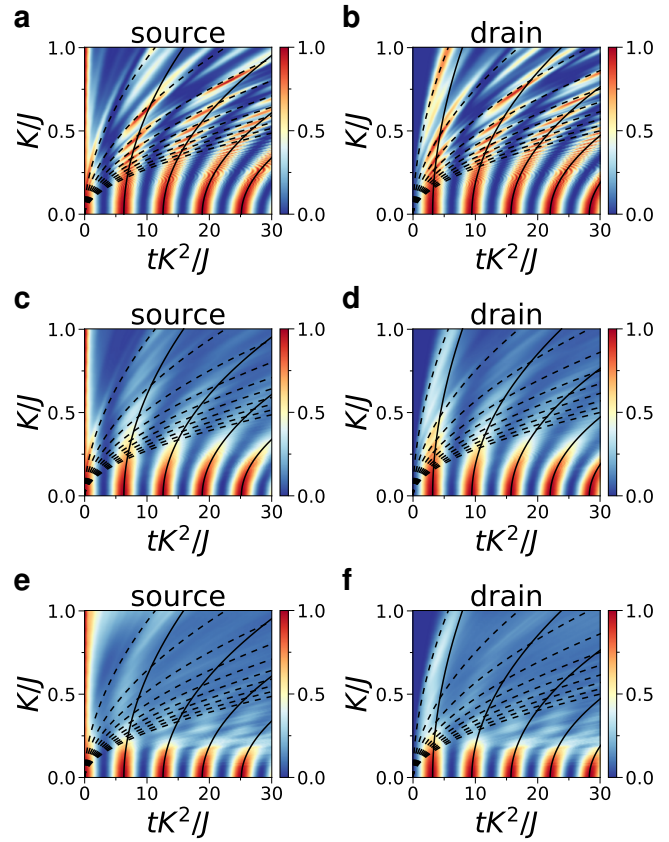


FIG. 13. Density in source and drain against K/J for $L/2 = 7$ and four particles with $U = 0$, $U/J = 1$ and $U/J = 5$ with analytic solution using Eq.A.15. For weak ring-lead coupling only one oscillation mode contributes, whereas for strong coupling additional oscillation modes are excited.

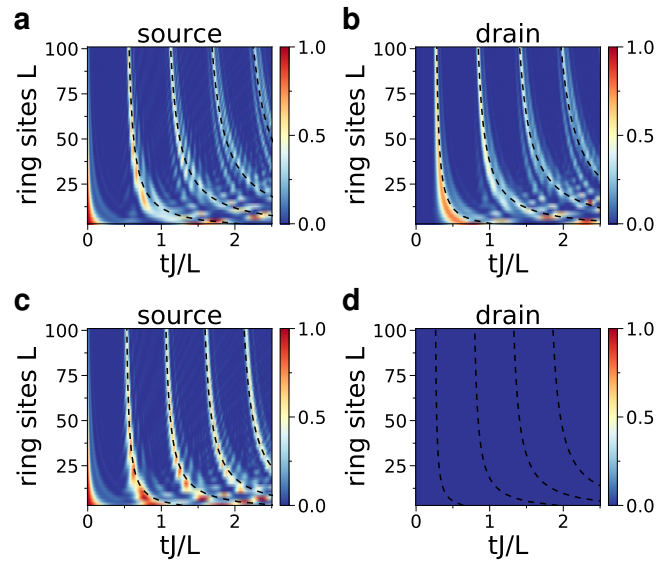


FIG. 14. Density in source and drain for $\Phi = 0$ and $\Phi = 0.5$. Dashed line is the analytic formula for strong coupling and large number of sites of Eq.A.17.

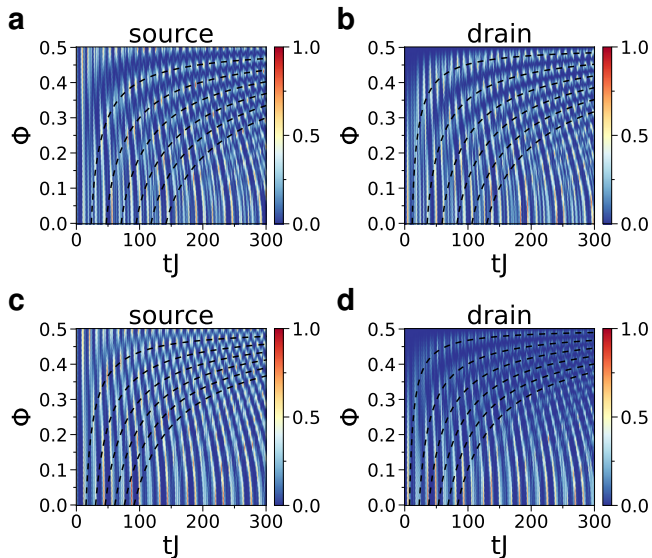


FIG. 15. Density in source and drain against flux for $K/J = 1$ and **a,b)** $L/2 = 7$ and **c,d)** $L/2 = 8$. Fit of $L/2 = 7$ with beating envelope calculated from Eq.A.14 and $L/2 = 8$ with Eq.A.8 and Eq.A.6.

metrically in the center of upper and lower arm of the ring, we can mimic the effect of flux on the oscillation periods. We plot the density in source and drain against Δ in Fig.16 without interaction and in Fig.17 with interaction. The oscillation frequency follows nearly the same relation as for flux, but no destructive interference is observed. This suggest we are not in the tunneling regime, and potential barriers and weak link play the role of scatters, and do not induce a simple phase shift.

Appendix: Quantum dot

To simulate the transport through a quantum dot inserted into the ring, the local potential in one arm of the ring is modified to a value Δ . The potential is modified on consecutive sites of the ring. This influences the rate with which particles are transported to the drain. The rate is calculated by integrating over the time evolution of the drain density over a long time. The result is seen in Fig.18. The plot shows the result without interaction, with interaction and as comparison the current in a open system driven by particle reservoirs at the leads for no interaction.

Appendix: Weak link

A weak link can be added into the system to modify the dynamics. The weak link is a modification of the coupling $J' = V$ between two specific sites in the center of one arm of the ring. We plot the dependence on the strength of a weak link V in Fig.19 for the strong-coupling regime. The weak link introduces characteristic beating frequencies.

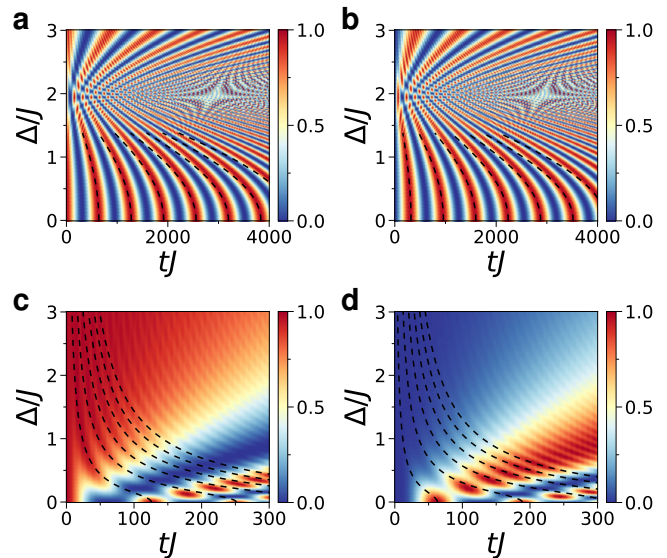


FIG. 16. Density in source and drain against two potential barriers in upper and lower arm of ring with strength Δ/J for **a,b)** $L/2 = 7$ and **c,d)** $L/2 = 8$. Other parameter are $K/J = 0.1$, $\Phi = 0$. The specific placement of the barriers has a strong impact on the dynamics. We choose a special placement which produced a behaviour which mimics the flux. For $L/2 = 8$, we place the barriers along the symmetry line through the center of ring, and for $L/2 = 7$, where there is no site on the symmetry axis, we choose the potential barrier such that the system remains point symmetric regarding the ring center. The fit uses the formulas for flux, but replaces $\Phi = \Delta/(2J)$ for $L/2 = 7$ and $\Phi = 2\Delta/(3J)$ for $L/2 = 8$. Note that there is an additional parity effect for $L/2 = 6, 10, 14, \dots$ which produces a different Δ dependency. The barriers act as a scattering impurity, which couple different momentum modes. Δ mainly changes the frequency of the density oscillation, but does not add any new additional oscillation frequencies. This means that the system is still dominated by one eigenmode. The scattering is only perturbing the overall dynamics, but not adding higher frequencies (in contrast to increasing ring-lead coupling K or adding more ring sites).

Appendix: Perfect state transfer

Now, we study the perfect state transfer scheme introduced in the main text in further detail. We plot flux Φ for the perfect state transfer scheme in Fig.20. For zero interaction, we see deterministic transfer between source and drain for $\Phi = 0$ with period $T = 1$. Close to $\Phi = 0.5$, the drain does not receive particles due to destructive interference in the ring. The oscillation time in source decreases here as the particles travel a shorter way as they cannot reach the drain. For intermediate Φ , we see beating patterns. This leads to a reemergence of the source population at some later time, e.g. for $\Phi = 0.3$ at $t/J = 7$. With Bose-Hubbard interaction, scattering leads to a smearing of the oscillation peaks.

We plot the flux dependence of the density in source and drain for the perfect state transfer scheme in Fig.21 for no interaction and mean-field interaction. With interaction, the oscillations become more regular. As long as the interaction

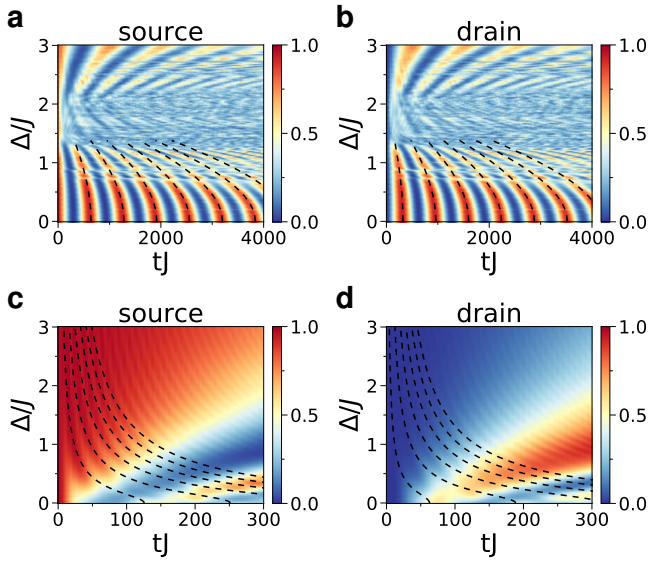


FIG. 17. Density in source and drain against two potential barriers in upper and lower arm of ring with strength Δ/J for **a,b**) $L/2 = 7$, $U/J = 3$ and **c,d**) $L/2 = 8$, $U/J = 1$. Other parameter are 4 particles, $K/J = 0.1$, $\Phi = 0$. The interaction washes out the faster dynamics, which has a larger ring population.

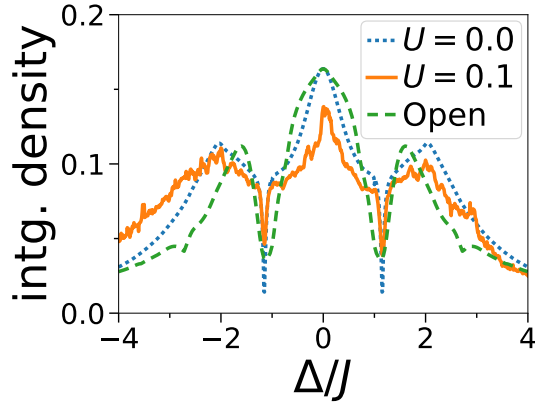


FIG. 18. Density in drain integrated over time $\Delta t = 10000/J$ when the local potential is Δ along one arm of the ring. Parameters are $K/J = 1$, $L/2 = 7$, 4 particles. Interference effects cause minima in transmission rate for certain values of Δ . For comparison, the dashed line shows the rescaled current for a non-interacting open system driven at the leads for the same configuration.

is in the dilute limit, perfect state transfer is still possible. However, for a non-dilute system scattering dilutes the perfect transfer.

Finally, we compare the perfect state transfer with no interaction with weak interaction (mean-field Gross-Pitaevskii) in Fig.22 for different values of flux. We notice that with interaction, the oscillation at $\Phi = 0.5$ are more regular compared to the non-interacting case.

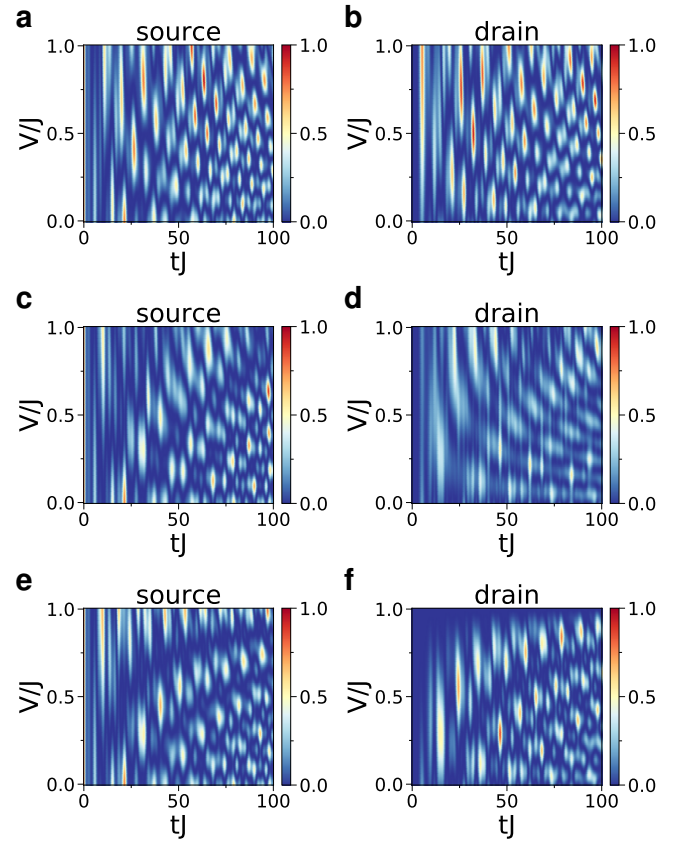


FIG. 19. Density in source and drain against tunneling rate of weak link V/J for $L/2 = 7$ and three particles with $\Phi = \{0, 0.35, 0.5\}$. The beating period changes its direction depending on the applied flux. Ring-lead coupling is $K/J = 1$.

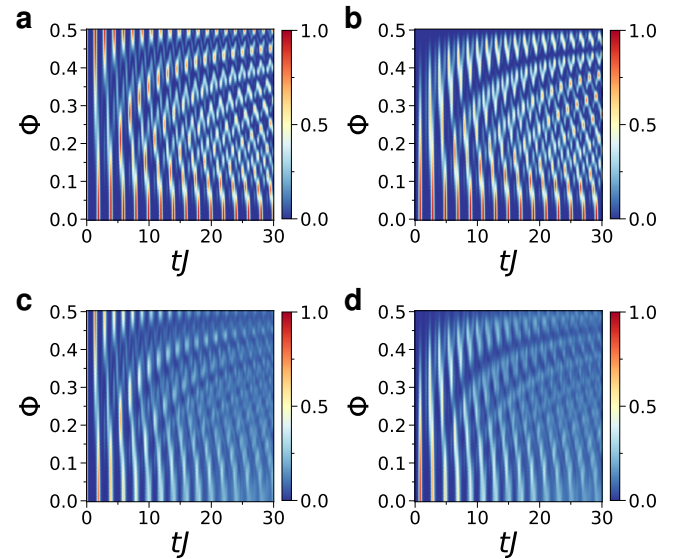


FIG. 20. Density in source and drain against Φ with couplings for perfect state transfer for $L/2 = 7$ and three particles with $U = 0$ and $U/J = 1$.

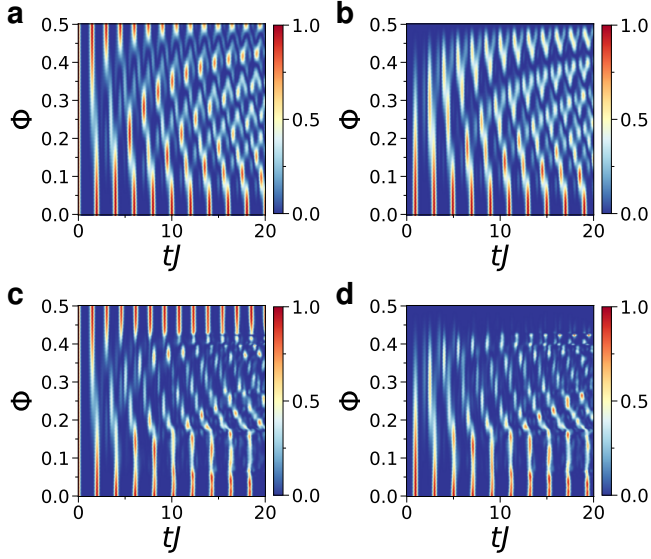


FIG. 21. Density in source **a,c**) and drain **b,d**), for $U = 0$ (**a,b**) and $U/J = 5$ (**c,d**). Number of ring sites $L/2 = 7$. Couplings are chosen for a perfect state transfer, such that for $\Phi = 0$ a particle in the source at $t = 0$ will be with unity probability in the drain at $t = 1$. The on-site interaction is the same in ring and leads. Calculation with Gross-Pitaevskii equation.

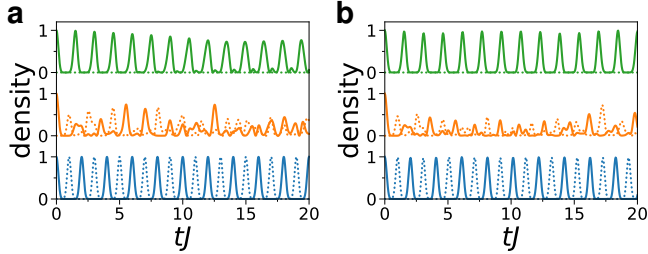


FIG. 22. **a**) Density in source (solid) and drain (dashed) with $UN/J = 0$ and $L = 14$. Couplings are chosen in a specific way such that for $\Phi = 0$ a particle in the source at $t = 0$ will be with unity probability in the drain at $t = 1$. From bottom to top $\Phi = \{0, 0.25, 0.5\}$. **b**) Comparison with interaction $UN/J = 5$. The on-site interaction is the same in ring and leads. Calculation with Gross-Pitaevskii.

Appendix: Interaction

In this section, we investigate the influence of on-site interaction on the time evolution. In Fig. 23, we compare the dynamics of the density in the source without and with interaction. We plot for the even parity the strong and weak coupling in Fig. 24. The density oscillation with interaction are plotted in Fig. 25. We observe oscillation with nearly the same frequency as in the non-interacting case, and additionally a varying envelope. The envelope decay increases with interaction and particle number, and can be fitted for intermediate time scales with a cosine. For certain values of flux, sharp resonances are observed with a faster decay.

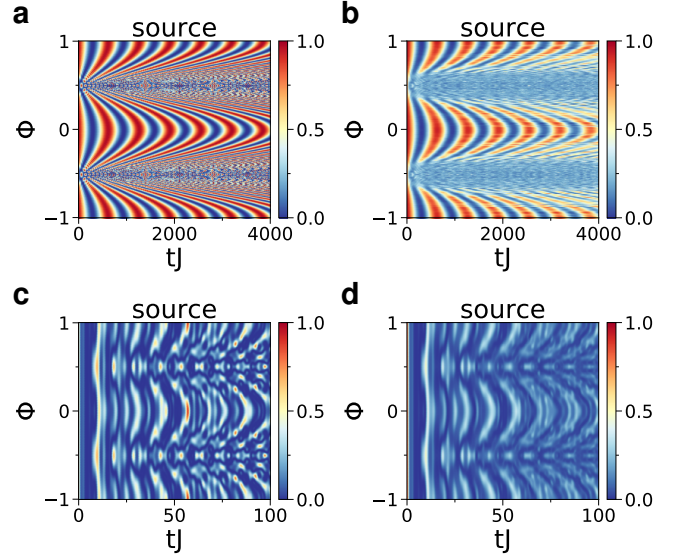


FIG. 23. Density in source against flux Φ for $L/2 = 7$ and 4 particles for weak coupling $K/J = 0.1$ **a**) $U = 0$ and **b**) $U/J = 0.2$ and strong coupling $K/J = 1$ **c**) $U = 0$ and **d**) $U/J = 5$.

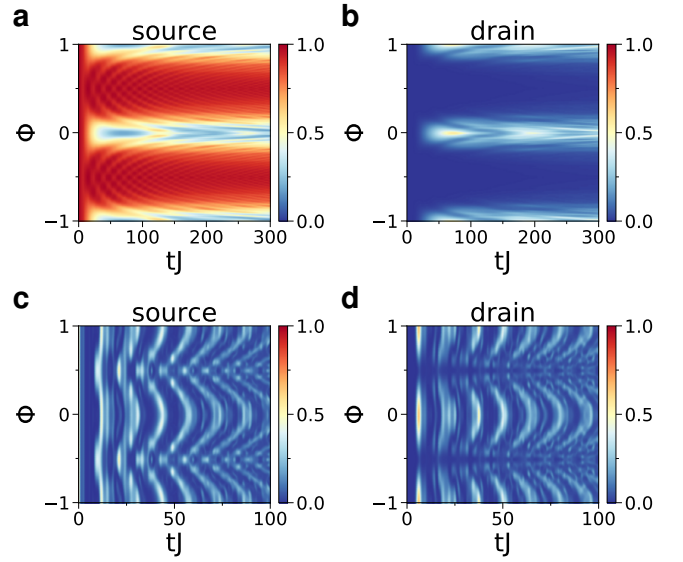


FIG. 24. Density in source **a,c**) and drain **b,d**) against flux Φ for $L/2 = 8$ and 4 particles for **a,b**) weak $K/J = 0.1$, $U = 1.0$ and **c,d**) strong coupling $K/J = 1.0$, $U = 0.2$.

Appendix: Open system

We study in this section the steady-state current through the ring driven by particle reservoirs at the leads. In Fig. 26, the current through the ring for a non-interacting system is plotted for large number of ring sites L . The current fits well with the transmission formula derived by Büttiker et al.[11]. We observe a good match especially in the weak coupling regime.

Next, we investigate the dependence of the steady-state current on the number of ring sites. We plot the current against

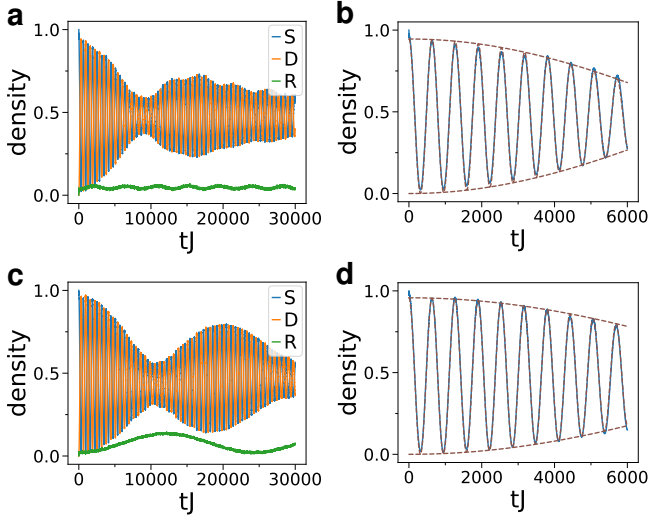


FIG. 25. **a)** Density in source, drain and ring for $L/2 = 5$, 5 particles, $K/J = 0.1$ and $U/J = 5$. **b)** Density in source fitted for shorter times with $f(t) = \frac{c}{2}(\cos(at)\cos(bt) + 1)$. Fitted parameters are $\{a = 1.866 \cdot 10^{-4}, b = 9.883 \cdot 10^{-3}, c = 9.455 \cdot 10^{-1}\}$. **c,d)** Same parameters and $L = 6$. Fitted parameters are $\{a = 1.472 \cdot 10^{-4}, b = 9.934 \cdot 10^{-3}, c = 9.577 \cdot 10^{-1}\}$.

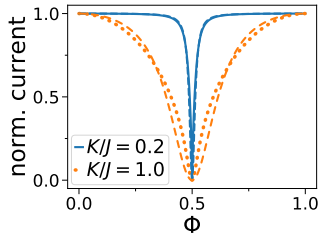


FIG. 26. Current through open system for no interaction with leads driven by particles reservoir plotted against flux Φ . Dashed line is a fit ($\epsilon = \{0.15, 0.49\}$) with transmission equation derived by Büttiker et al.[11]. Numerical calculation of open system with formalism of third quantization [36] and $L = 100$.

flux for weak and strong coupling and various number of ring sites L in Fig.27. The two parities ($L/2 = 3, 5, \dots$ and $L/2 = 2, 4, \dots$) have different flux dependence, which is especially pronounced in the weak coupling limit $K/J \ll 1$ and for smaller number of ring sites L . For many ring sites the parity effect vanishes. In Fig.28, we investigate the dependence of the steady-state current on flux and the filling factor in the leads.

In Fig.29 we plot the current through the rings against the statistics η and the applied flux Φ for infinite strong on-site repulsion. We observe a minimum of the current except at $\eta = \pm 1$. The suppression of the current for fermionic $\eta = 0$ is due to the Aharonov-Bohm effect. The flux-dependence vanishes for interacting bosons at $\eta = 1$ [30]. The current for weak coupling is plotted in Fig.30. More lines are visible, which may be related to many-body resonances. We study the difference of weak and strong coupling with the parity ef-

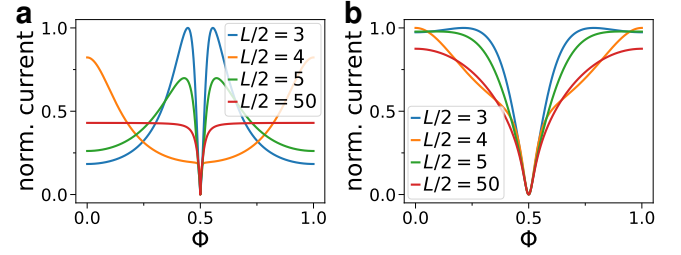


FIG. 27. Current through non-interacting ring with driven leads against flux Φ . Different number of ring sites for **a)** weak-coupling ($K/J = 0.2$) and **b)** strong coupling regime ($K/J = 1.0$). Even and odd parity has different dependence on flux. It is best seen for weak ring-lead coupling and for small number of sites. It vanishes for $L \gtrsim 100$.

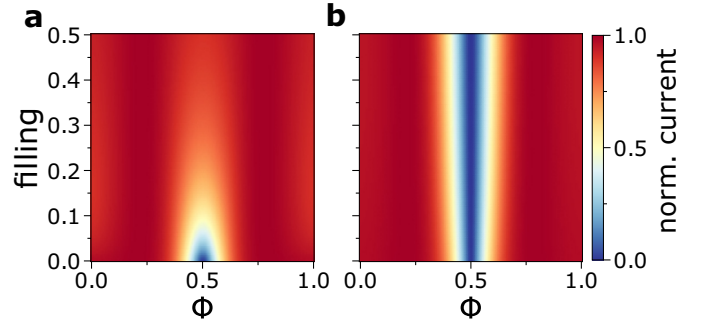


FIG. 28. Steady-state current through ring with flux Φ and filling factor for **a)** hard-core bosons and **b)** fermions for $L/2 = 3$ and strong coupling $K/J = 1$ ($\eta = \{0, 2\}$). The Aharonov-Bohm effect for low filling corresponds to the fermionic case, but vanishes for hard-core bosons for higher filling factor. Fermions are nearly unaffected by filling. Only a weak bias difference in filling of $\Delta n = 0.01$ is applied. The driving strength is $\Gamma = 0.5$. The current is normalized to the maximum for each value of filling.

fect for different types of particles in Fig.31. For weak coupling, the parity has a pronounced effect on the Aharonov-Bohm effect, shifting the maximum of the steady-state current. The parity effect is suppressed for strong coupling. We observe that for hard-core bosons the flux dependence is

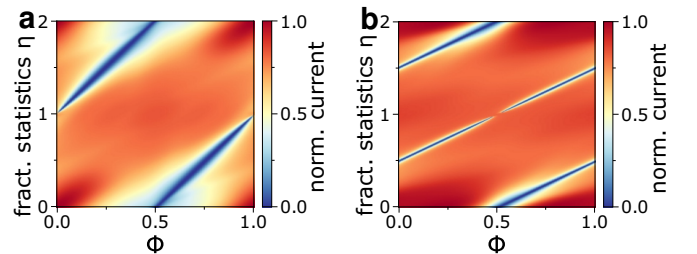


FIG. 29. Steady-state current through ring with flux Φ and fractional statistics η ($\eta = \{0, 2\}$ non-interacting fermions, $\eta = 1$ hard-core bosons) for strong coupling $K/J = 1$. Number of sites of ring are **a)** $L/2 = 2$ and **b)** $L/2 = 3$. Other parameter are $\Gamma = 0.5$ and $f = 1$.

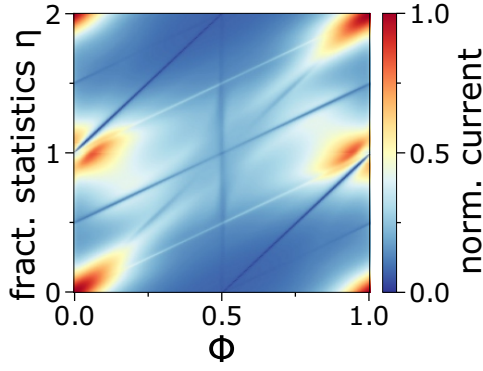


FIG. 30. Steady-state current through ring with flux Φ and fractional statistics η ($\eta = \{0, 2\}$ non-interacting fermions, $\eta = 1$ hard-core bosons) for weak coupling $K/J = 0.2$. Other parameters are $\Gamma = 0.5$, $f = 1$, $L/2 = 2$.

nearly flat only for strong coupling, whereas there is still a visible Aharonov-Bohm effect in weak coupling.

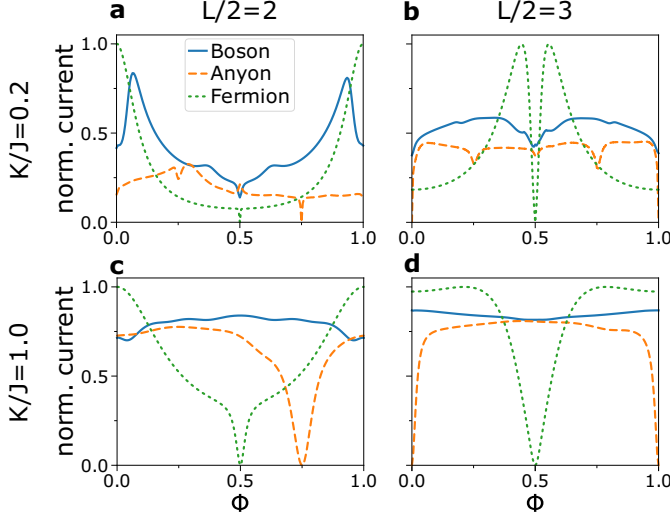


FIG. 31. **a-d**) Steady-state current for weak and strong coupling for odd and even parity with hard-core bosons, fermions and anyons ($\eta = 0.5$). The on-site interaction is infinite both in leads and ring. Fermions and anyons have zero current at a specific flux, whereas for interacting bosons the current is nearly constant and the Aharonov-Bohm effect suppressed. The anyon statistics shift the minimum of the Aharonov-Bohm interference as the commutation relations introduce an effective flux, which depends on the average number of particles in ring and therefore the number of ring sites. The steady-state current operator is $j = -iK(\hat{a}_s^\dagger \hat{a}_0 - \hat{a}_0^\dagger \hat{a}_s)$. The expectation value is calculated as $\langle j \rangle = \text{Tr}(j\rho)$ with ρ being the steady state density matrix. The leads are incoherently coupled to a particle reservoir at the leads with a population imbalance between source and drain. The coupling is assumed to be weak and within the Born-Markov approximation, modeled with the Lindblad Master-equation and strong source-drain imbalance ($f = 1$) and driving $\Gamma = 0.5$.

The position of minimal current depends on the length of the ring L and the fractional statistics η as seen in Fig. 29a ($L/2 = 2$) and Fig. 29b ($L/2 = 3$). For specific value of flux,

the current becomes zero. For infinite on-site interaction U it is given by the degeneracy point of a half-filled ring. The fractional statistics has the role of an effective flux, and the degeneracy point and minimal current is at flux

$$\Phi_{\min} = \eta \frac{L-2}{4} + \frac{1}{2}. \quad (\text{A.3})$$

For $\eta = 1$ (hard-core bosons), the equation is not valid anymore, as there is a discontinuity with non-zero current. The formula itself can be explained by the following: A ring is formed when first and last site of a chain are linked together. At that position, the numbering of sites changes. Whenever a particle hops across this point of the ring, it commutes with all the particles at the remaining $L - 2$ sites. In the driven setup, the ring is half-filled, thus there are on average $(L - 2)/2$ particles on those sites. The phase shift (or effective flux) due to the commutation rules is then $\eta\pi(L - 2)/2$, adding to the phase shift induced by the flux.

Appendix: Non-interacting solutions

To investigate the Hamiltonian, it is convenient to write the ring Hamiltonian in Fourier space (for $U = 0$)

$$\mathcal{H} = \sum_{j=0}^{L-1} -2J \cos\left(\frac{2\pi}{L}(j - \Phi)\right) \hat{b}_j^\dagger \hat{b}_j + \sum_{j=0}^{L-1} \frac{K}{\sqrt{L}} \left(\hat{a}_s^\dagger \hat{b}_j + (-1)^j \hat{a}_D^\dagger \hat{b}_j + \text{H.C.} \right), \quad (\text{A.4})$$

where \hat{b}_j the Fourier transform of the annihilation operator of the ring.

In the following, we assume that all the particles are initially loaded into the source. We investigate the dynamics for weak coupling $K \ll J$ or for small number of ring sites L . The time evolution governed by the eigenmodes $|\Psi_j\rangle$ with energy E_j . It is given by $|\Psi(t)\rangle = \sum_j e^{-iE_j t} |\Psi_j\rangle \langle \Psi_j | \Psi(0)\rangle$. Due to the symmetry of the system, the spectrum has pairs of eigenvalues $\pm E_j$ and the corresponding eigenvectors of each pair have the same absolute value for drain and source. Using these properties, we can write the dynamics for the density in source n_S in terms of the coefficient of the eigenvalue at source and drain A_j as follows

$$n_S(t) = \left| \sum_{j \in \text{pairs}} \cos(E_j t) |A_j|^2 \right|^2$$

and the drain density n_D for odd parity

$$n_D(t) = \left| \sum_{j \in \text{pairs}} (-1)^j \sin(E_j t) |A_j|^2 \right|^2$$

and for even parity

$$n_D(t) = \left| \sum_{j \in \text{pairs}} (-1)^j \cos(E_j t) |A_j|^2 \right|^2.$$

In the weak coupling limit $K \ll J$ or for small number of ring sites L , the dynamics can be described by an effective, reduced system, consisting of source, drain and a small number of ring eigenmodes L_0 . With above equation, the dynamics is then given by the sum over the $L_0/2 + 1$ eigenmode pairs of the reduced system.

We justify this method as follows: Initially, all particles are prepared in the source and a total energy $E = 0$. Source and drain are coupled via the ring eigenmodes. Coupling is most efficient if the energy difference between the modes is small, thus the leads will couple mainly to the ring eigenmodes with energy close to the leads.

We identify two mechanism for transport through the ring: Firstly, resonant coupling to ring eigenmodes with energies close to that of the uncoupled leads. A similar concept is known as resonant tunneling in quantum dots. Secondly, off-resonant coupling enhanced by interference via all ring modes with energies not too close to the leads. Which mechanism is important depends on L and can be grouped into two distinct parities $L/2$ even and odd. For even parity, the second mechanism is not possible as it turns out the ring modes destructively interfere for any value of Φ . Thus, transport is dominated by resonant coupling to ring eigenmodes $E \approx 0$. For odd parity, both mechanisms contribute. For $\Phi \approx 0$, off-resonant coupling is dominant, while for $\Phi \approx \frac{1}{2}$ resonant coupling. The difference in both parities arises from two effects: First, different eigenmode distributions. E.g. for even parity and $\Phi = 0$ there are two ring modes with eigenvalue zero, whereas for odd parity this is not the case. For $\Phi = 0.5$, the two cases interchange and the opposite is true.

Secondly, interference of ring modes at the ring-drain coupling. The eigenvalues can be grouped into pairs with the same absolute value, but opposite sign $\pm E$. They have the momentum mode number $n_- = n$ and $n_+ = n + \frac{L}{2}$. As seen in Eq.A.4, the sign of the ring-drain coupling depends on the momentum mode number. For even parity, the eigenvalue pairs $\pm E$ have the same sign for the ring-drain coupling, whereas for odd the coupling has opposite signs. This has a profound effect on the dynamics. For even parity, the eigenmode pair $\pm E$ will interfere destructively in the drain, while for odd constructively. This effect is independent of Φ . Note that when the ring modes couple strongly with the leads, the interference condition is relaxed. Thus, this argument is only valid for off-resonant coupling. Both descriptions break down in the strong-coupling limit and for a large number of sites as more and more ring eigenmodes couple to the leads as the energy spacing between ring modes decreases.

Next, we describe how to calculate the eigenvalues of ring-lead system. We write down the eigenvalue equation with the Hamiltonian of Eq.A.4 for noninteracting particles $\hat{H}|\Psi\rangle = E|\Psi\rangle$ for an arbitrary eigenstate $|\Psi\rangle = \alpha_S|S\rangle + \alpha_D|D\rangle + \sum_{n=0}^{L-1} \alpha_n|n\rangle$, where α_S is the coefficient of the source site, α_D of the drain, and α_n of ring eigenmode n . We get $L + 2$

equations for the coefficients

$$\begin{aligned} E\alpha_S &= \frac{K}{\sqrt{L}} \sum_{n=0}^{L-1} \alpha_n \\ E\alpha_D &= \frac{K}{\sqrt{L}} \sum_{n=0}^{L-1} (-1)^n \alpha_n \\ E\alpha_n &= -2J \cos\left(\frac{2\pi(n-\Phi)}{L}\right) \alpha_n + \frac{K}{\sqrt{L}} (\alpha_S + (-1)^n \alpha_D). \end{aligned}$$

We insert the equations for α_n into the source and drain equations

$$\begin{aligned} E\alpha_S &= \frac{K^2}{2JL} \sum_{n=0}^{L-1} \frac{\alpha_S + (-1)^n \alpha_D}{\frac{E}{2J} + \cos\left(\frac{2\pi(n-\Phi)}{L}\right)} \\ E\alpha_D &= \frac{K^2}{2JL} \sum_{n=0}^{L-1} \frac{(-1)^n \alpha_S + \alpha_D}{\frac{E}{2J} + \cos\left(\frac{2\pi(n-\Phi)}{L}\right)}. \end{aligned} \quad (\text{A.5})$$

Using these two equations as starting point, we can make approximations. We define $\tilde{K} = K/J$.

For resonant coupling, we keep only the dominant terms of the sum in Eq.A.5. E.g. for odd parity and $\Phi \approx 0.5$ they are $n = \frac{L+2}{4}$ and $n = \frac{3L+2}{4}$, and for even parity and $\Phi \approx 0$ $n = \frac{L}{4}$ and $n = \frac{3L}{4}$. The resulting eigenvalues for even parity are

$$E = 0, \quad E/J = 2 \sqrt{\sin\left(\frac{2\pi\Phi}{L}\right)^2 + \left(\frac{\tilde{K}}{\sqrt{L}}\right)^2}, \quad (\text{A.6})$$

and for odd

$$E_{\pm}/J = \sin\left(\frac{2\pi(\Phi - 0.5)}{L}\right) \pm \sqrt{\sin\left(\frac{2\pi(\Phi - 0.5)}{L}\right)^2 + \left(\frac{\sqrt{2}\tilde{K}}{\sqrt{L}}\right)^2}. \quad (\text{A.7})$$

The equations are quite different for each parity as the sign of the ring-lead coupling depends on the parity as well.

For even parity and $\Phi \approx 0.5$, the source oscillations disappear in the weak-coupling limit. Interestingly, for strong coupling we still find density oscillations and we observe a characteristic beating. To calculate, we have to include in total four wavenumbers ($n = \frac{L}{4}$, $n = \frac{L+4}{4}$, and $n = \frac{3L}{4}$, $n = \frac{3L+4}{4}$) as at this flux all these ring modes have nearly the same energy. We get the same eigenvalues as in Eq.A.6 and additionally

$$E/J = 2 \sqrt{\sin\left(\frac{2\pi(\Phi - 1)}{L}\right)^2 + \left(\frac{\tilde{K}}{\sqrt{L}}\right)^2}. \quad (\text{A.8})$$

The beating frequency is given by the subtraction of these eigenvalues and Eq.A.6.

In the other limit $\Phi \approx 0$ and $K/J \approx 1$ or $L \gg 1$, a higher frequency mode appears in the density oscillation. To calculate, we include in total six wavenumbers ($n = \frac{L}{4}$, $n = \frac{L+4}{4}$, $n = \frac{L-4}{4}$, and $n = \frac{3L}{4}$, $n = \frac{3L+4}{4}$, $n = \frac{3L-4}{4}$). We get the original eigenvalue of Eq.A.6 and two new ones, of which only the

following has a non-negligible contribution A_j to the source and drain dynamics

$$E/J = \left[\left(\frac{2\tilde{K}}{\sqrt{L}} \right)^2 + 2 \left(1 - \cos\left(\frac{4\pi}{L}\right) \cos\left(\frac{4\pi\Phi}{L}\right) \right) + \left\{ \left(\frac{2\tilde{K}}{\sqrt{L}} \right)^4 + \left(1 + \cos\left(\frac{8\pi}{L}\right) \cos\left(\frac{8\pi\Phi}{L}\right) - \cos\left(\frac{8\pi}{L}\right) - \cos\left(\frac{8\pi\Phi}{L}\right) \right\}^{\frac{1}{2}} \right]^{\frac{1}{2}}. \quad (\text{A.9})$$

This equation is not valid for small L and $\Phi \approx 0.5$.

Next, we show how to calculate off-resonant contributions. In the weak-coupling limit, we assume that the eigenenergy E will be close to the energy of the uncoupled leads $E = 0$. Thus, we perform a Taylor expansion of the fraction around $E = 0$

$$\frac{1}{\frac{E}{2J} + \cos\left(\frac{2\pi(n-\Phi)}{L}\right)} = \sum_{p=0}^{\infty} \left[-\frac{E}{2J} \sec\left(\frac{2\pi(n-\Phi)}{L}\right) \right]^p. \quad (\text{A.10})$$

The eigenvalue equation becomes

$$E\alpha_S = \frac{K^2}{2JL} \sum_{p=0}^{\infty} \left(\frac{-E}{2J} \right)^p (\beta_p^+ \alpha_S + \beta_p^- \alpha_D) \quad (\text{A.11})$$

and analog for $E\alpha_D$ with $\beta_p^+ = \sum_{n=0}^{L-1} \sec\left(\frac{2\pi}{L}(n-\Phi)\right)^p$ and $\beta_p^- = \sum_{n=0}^{L-1} (-1)^n \sec\left(\frac{2\pi}{L}(n-\Phi)\right)^p$. The coefficients reveal the parity effect. For even parity and all values of Φ , β_p^+ is either zero or infinity, and β_p^- is always zero. Thus, off-resonant coupling can be neglected for any order of p for even parity. For odd parity, we have $\beta_p^+ = 0$ for $p \in \text{even}$ and $\beta_p^- = 0$ for $p \in \text{odd}$. Two exact solutions are known to us $\beta_0^- = \pm \frac{L}{\cos(\Phi\pi)}$ and $\beta_1^+ = \frac{L^2}{2\cos(\Phi\pi)^2}$. For a simple zero order expansion of all modes, without resonant tunneling (valid for $\Phi \approx 0$), the density oscillation has the frequency

$$E/J = \frac{\tilde{K}^2}{|\cos(\Phi\pi)|}. \quad (\text{A.12})$$

It is possible to also derive higher order versions of this equation for increased accuracy. First order yields

$$E/J = \frac{4\tilde{K}^2 \cos(\Phi\pi)}{8\cos(\Phi\pi)^2 + 2L\tilde{K}^2}. \quad (\text{A.13})$$

It is possible to combine resonant and off-resonant coupling. One has to apply the method for resonant coupling, and use the off-resonant method for all other eigenmodes minus the resonant ones. The sum over n has to be adjusted accordingly. The result for order $p = 0$ is

$$E_{\pm}/J = \pm \left[\frac{\tilde{K}^2}{2L \sin\left(\frac{\pi}{L}(1-2\Phi)\right)} - \frac{\tilde{K}^2}{4\cos(\Phi\pi)} + \sin\left(\frac{\pi}{L}(1-2\Phi)\right) \right] + \left[\left(\frac{\tilde{K}^2}{2L \sin\left(\frac{\pi}{L}(1-2\Phi)\right)} - \frac{\tilde{K}^2}{4\cos(\Phi\pi)} + \sin\left(\frac{\pi}{L}(1-2\Phi)\right) \right)^2 + \frac{\tilde{K}^2 \sin\left(\frac{\pi}{L}(1-2\Phi)\right)}{\cos(\pi\Phi)} \right]^{\frac{1}{2}}. \quad (\text{A.14})$$

and for order $p = 1$ we get with $\delta = \csc\left(\frac{\pi}{L}(1-2\Phi)\right)$ and $\gamma = \sec(\Phi\pi)$

$$E_{\pm}/J = \pm \frac{L}{\delta} \frac{8 + \tilde{K}^2 L \gamma^2 - 2\tilde{K}^2 \delta \gamma}{4\tilde{K}^2 \delta^2 - L(8 + \tilde{K}^2 L \gamma^2)} + \left[\left(\frac{L}{\delta} \frac{8 + \tilde{K}^2 L \gamma^2 - 2\tilde{K}^2 \delta \gamma}{4\tilde{K}^2 \delta^2 - L(8 + \tilde{K}^2 L \gamma^2)} \right)^2 + \frac{L}{\delta} \frac{8\tilde{K}^2 \gamma}{8L + \tilde{K}^2 (L^2 \gamma^2 - 4\delta^2)} \right]^{\frac{1}{2}}. \quad (\text{A.15})$$

So far, we only discussed the eigenvalues, which represent the frequency of the oscillation in source and drain. As outlined in the beginning of the section it can be described by a superposition of Cosines with the relevant eigenvalues of the reduced system. Now, we discuss the relative strength of the Cosine contribution A_{\pm} , which is the coefficient of the eigenvector in drain and source. For resonant coupling, we can write down the reduced Hamiltonian and solve for the eigenvectors and calculate A_j . For off-resonant, writing down the reduced Hamiltonian is not so trivial. Using numerics, we established that for odd parity and $\Phi \approx 0$, E_+ dominates and only a minor contribution of E_- contributes for larger ring lengths. For $\Phi \approx 0.5$, both frequencies contribute equally, and a beating between the frequency occurs.

For strong coupling $K \approx J$ and many ring sites $L \gg 1$, we can define a ballistic model. We split the propagation into two separate parts: A Rabi oscillation between lead and neighboring ring site, and the subsequent propagation inside the ring with the group velocity of the bare ring. The lead-ring interaction couples to all wavenumber modes equally, creating two wavepackets in clockwise and anti-clockwise direction. The central wavenumbers in each packet are $n = \pm L/4$, and the resulting group velocity v

$$v = \frac{\partial E}{\partial k} = 2J \sin \frac{2\pi n}{L} = 2J. \quad (\text{A.16})$$

The time for one oscillation between source - drain - source is given by

$$T_{\Phi=0} = \frac{L}{2J} + \frac{2\pi}{K} \\ T_{\Phi=0.5} = \frac{L}{2J} + \frac{\pi}{K}. \quad (\text{A.17})$$

The time for $\Phi = 0.5$ is shorter as the particles destructively interfere and thus do not propagate into the drain.

Finally, we investigate the equations for a weak link in the ring. In the case of a very strong weak link, reducing at a

single point J to zero, we can solve the equations. In this case, the ring becomes an open chain. The momentum modes are $k_n = \frac{\pi n}{L+1}$ with $n = 1 \dots L$ and the new Fourier transform $\hat{b}_k = \sqrt{\frac{2}{L+1}} \sum_{n=1}^L \sin(kn) \hat{a}_n$. The resulting Hamiltonian can be made independent of flux as it can be absorbed into the definition of the ring operators. Repeating the steps for the ring results for weak coupling in similar equations. We place the weak link on the symmetry axis between source and drain in one of the ring arms. Using the approximation of $E = 0$ in the fraction reveals a new parity effect: We get eigenvalue zero for all number of ring sites except $L/4$ odd. Except in that case there are no drain and source oscillations, and the drain is always empty. For $L/4$ odd we observe oscillations with two times the frequency of the full ring $E/J = 2\tilde{K}^2$.

Appendix: Potential in ring

The local potential of the ring sites can be modified by the optical trapping field. The ring Hamiltonian becomes

$$\mathcal{H}_r = \sum_{j=0}^{L-1} \left(-J e^{i2\pi\Phi/L} \hat{a}_j^\dagger \hat{a}_{j+1} + \text{H.C.} \right) + \sum_{j=0}^{L-1} \hat{n}_j \left[\frac{U}{2} (\hat{n}_j - 1) + \Lambda_j \right] \quad (\text{A.18})$$

with Λ_j the local potential at site j . We investigate two different realizations: a configuration with a potential barrier, and one with a quantum dot: In the first, we modify the potential at one site with $\Lambda_j = \Delta$ in each arm of the ring and at all other sites $\Lambda_j = 0$. This realizes a configuration with two potential barriers. In detail, we choose $j = \text{ceil}(\frac{1}{4L}) - 1$ and $j = \text{ceil}(\frac{3}{4L}) - 1$. This configuration allows to control the oscillation period between source and drain in the weak-coupling limit. The functional relationship is very similar to the flux through the ring.

In the second, we change the potential to a non-zero value $\Lambda_j = \Delta$ in one arm over several consecutive sites. The exact placement and length of the quantum dot has a distinct influence on the transmission. Specifically, we choose $j = \{0, \dots, \frac{L-4+\text{mod}(L,4)}{2}\}$.

Appendix: Engineering perfect state transfer

By choosing the inter-site tunneling parameter J with certain site-dependent values, particles can be deterministically transferred with unity probability [33]. E.g. a particle initially placed in the source will be with unity probability at time $t = \frac{1}{J}$ in the drain, and subsequently oscillate with constant frequency between both. The tunneling parameters are

$$J_n = \frac{\pi}{2} J \sqrt{s_n} \sqrt{n(L_0 - n)} \quad (\text{A.19})$$

where L_0 is the number of sites of the path between source and drain and s_n a modifier at junctions to fulfill Kirchoff's law ($\sum s_n^{\text{in}} = \sum s_n^{\text{out}}$). At a junction, e.g. the ring site which couples

to drain and two other ring site, we get $s_n = 0.5$ towards the two other ring sites and $s_n = 1$ towards the drain. At regular sites with only couplings to two other sites we have $s_n = 1$.

Appendix: Open ring-lead system

In an open system, the ring-lead configuration is coupled to external reservoirs. An external source and sink of particles couples to the source and drain sites, adding and removing particles only at the lead sites. The ring itself does not interact with the reservoir directly. The model is adapted from fermions in a 1D chain[37]. The coupling between the leads and the reservoir is weak, so that the state of the system ρ consisting of ring and leads can be written independently of the reservoir $\rho_{\text{total}} = \rho \otimes \rho_{\text{reservoir}}$.

The driving term is modeled with the Lindblad master equation

$$\frac{\partial \rho}{\partial t} = -\frac{i}{\hbar} [H, \rho] - \frac{1}{2} \sum_m \{ \hat{L}_m^\dagger \hat{L}_m, \rho \} + \sum_m \hat{L}_m \rho \hat{L}_m^\dagger, \quad (\text{A.20})$$

\hat{L}_m the Lindblad operator which describes the action of the reservoir on the leads, and $[\cdot, \cdot]$ ($\{\cdot, \cdot\}$) is the commutator (anti-commutator). We investigate two types of reservoir-lead interaction by the Lindblad operators. A fermionic type of driving

$$L_1 = \sqrt{\Gamma \frac{1+f}{2}} \hat{a}_S^\dagger, \quad L_2 = \sqrt{\Gamma \frac{1-f}{2}} \hat{a}_S \\ L_3 = \sqrt{\Gamma \frac{1-f}{2}} \hat{a}_D^\dagger, \quad L_4 = \sqrt{\Gamma \frac{1+f}{2}} \hat{a}_D,$$

with Γ the reservoir-lead coupling and $f \in \{0, 1\}$ the imbalance between source and drain reservoir occupation. For all f , the system is close to half-filling. For $f = 1$, the source reservoir only emits and the drain reservoir only receives particles.

For a bosonic type of driving, we choose the following definition

$$L_1 = \sqrt{\Gamma n_S} \hat{a}_S^\dagger, \quad L_2 = \sqrt{\Gamma (n_S + 1)} \hat{a}_S \\ L_3 = \sqrt{\Gamma n_D} \hat{a}_D^\dagger, \quad L_4 = \sqrt{\Gamma (n_D + 1)} \hat{a}_D,$$

with n_S and n_D the average occupation number of the uncoupled source and drain, called filling in the main text. With increasing n_S , the ring becomes more filled. The difference between n_S and n_D is defined as Δn .

Note that in case the lead site is occupied, the interaction energy on-site has to be provided by the reservoir, which may change the coupling strength. In the following, we assume that the Lindblad term is independent of the on-site interaction energy.

From the continuity equation we define the current at the source

$$j_S = -iK(\hat{a}_S^\dagger \hat{a}_0 - \hat{a}_0^\dagger \hat{a}_S) \quad (\text{A.21})$$

and at the drain

$$j_D = -iK(\hat{a}_{L/2}^\dagger \hat{a}_D - \hat{a}_D^\dagger \hat{a}_{L/2}). \quad (\text{A.22})$$

In the steady state limit, both currents are identical.

We assume fractional statistics as a generalization of fermion and bosons [38]

$$\begin{aligned} \hat{a}_n^\dagger \hat{a}_m + q_{m,n} \hat{a}_m \hat{a}_n^\dagger &= \delta_{m,n} \\ \hat{a}_n \hat{a}_m + q_{m,n}^{-1} \hat{a}_m \hat{a}_n &= 0. \end{aligned}$$

where $q_{m,n}$ define the fractional statistics. We choose following implementation with $q \in \mathbb{C}$

$$q_{m,n} = \begin{cases} q, & m > n \\ \pm 1, & m = n \\ q^{-1}, & m < n \end{cases} \quad (\text{A.23})$$

$$(\text{A.24})$$

$$(\text{A.25})$$

We define the parameter η with $q = e^{i\pi\eta}$. For $\eta = 0$, we retain the fermionic anticommutator, while for $\eta = 1$ the bosonic commutation rules. For the case $m = n$, we can choose to either enforce the Pauli exclusion principle $p_{m,m} = 1$ or allow multiple particles per site $p_{m,m} = -1$. For $\eta \neq 1$ we use the Jordan-Wigner transformations to map the Hamiltonian from bosonic commutation rules to fractional statistics. When a particle changes the position to a non-consecutive site number, the particle assumes a phase factor for every passed particle. The Jordan-Wigner transformation expresses this phase

factor by a non-local interaction. Note that the explicit form depends only on the arbitrary numbering of the sites, not the actual position in real space. The Jordan-Wigner transformation for hopping from m to n , is given by

$$\hat{a}_n^\dagger \hat{a}_m \rightarrow \hat{a}_n^\dagger \hat{a}_m \prod_{j=m+1}^{n-1} e^{i\pi(1-\eta)\hat{n}_j \text{sgn}(m-n)}. \quad (\text{A.26})$$

In the following, we allow only one particle per site ($q_{m,m} = 1$). For the fermionic case, this is the Pauli-principle, while for bosons this corresponds to the hard-core boson model with infinite on-site interaction U . We map the problem to a spin-model with Pauli-matrices. In this case, the open system Hamiltonian for infinite repulsion is

$$\mathcal{H} = - \sum_{j=0}^{L-1} \left(J e^{i2\pi\Phi/L} \sigma_j^+ \sigma_{j+1}^- \right) - K \left(\sigma_S^+ \sigma_0^- + \sigma_D^+ \sigma_{L/2}^- \right) + \text{H.C.} \quad (\text{A.27})$$

Additionally, the Jordan Wigner transformation has to be applied for the hopping terms according to the chosen enumeration of the sites. The current operator requires the same treatment.

To solve the equations, we initialize the system in a random state, then evolve it in time until the steady state is reached. By solving the open system exactly [36, 39] we confirmed that non-interacting fermions and bosons have the same flux dependence.